JOURNAL OF MATERIALS SCIENCE 30 (1995) 4973–4979

Hydrogen activation of $LaNi_5$: Implications of fracture mechanisms on hydriding properties

T. KASTRISSIOS, E. KISI*, S. MYHRA
Faculty of Science and Technology, Griffith University, Nathan, Queensland 4111, Australia

The fracture mechanisms of two different $LaNi_5$ alloys (A and B) have been investigated during the first few hydrogen loading/unloading cycles that constitute activation of this material. The principal difference between the two formulations was the presence of Ni-deficient planar inclusions, oriented perpendicular to the crystallographic *c*-axis, in alloy A. Both types were found to fracture at high loadings of hydrogen (hydrogen-to-metal ratios of ca. 1) during the activation cycle, as a result of the differential expansion between the microdomains of the α- and β-hydride phases. However, alloy A also fractured at an earlier stage in the activation cycle, at very low hydrogen-to-metal ratios (≤ 0.06), by delamination at the planar inclusion boundaries. This had the effect of reducing the hysteresis during the first activation cycle, most probably due to faster kinetics. The implication is that the hydrogen storage properties of the alloy can be tailored by microstructural design.

1. Introduction

The intermetallic alloy $LaNi_5$ is known to absorb hydrogen at room temperature and ca. 2×10^5 Pa pressure following activation at high pressure. It has the capacity to absorb about six hydrogen atoms per formula unit to form the concentrated β-phase hydride ($LaNi_5H_6$) [1]. The merits of $LaNi_5$ include high storage capacity, ease of recovery of the hydrogen near 1×10^5 Pa and room temperature, moderate stability of the reaction products and good resistance to poisoning. Favourable kinetics and constancy of the equilibrium pressure during the reaction at constant temperature are also attractive properties for technical applications.

The system is hysteretic, i.e. it has non-equivalent absorption and desorption isotherms in the pressure–composition diagrams. This has been attributed to the $\alpha \leftrightarrow \beta$ phase transformation, and is thought to originate from either the generation of defect structures during plastic deformation [2] or oversaturation of the α-phase on absorption and undersaturation of the β-phase on desorption during which H–H correlations and interaction energies between the hydrogen atoms in the lattice play major roles [3].

$LaNi_5$ requires activation at high pressures before it can readily absorb hydrogen (i.e. become a hydridable alloy). This is achieved by cycling hydrogen into and out of $LaNi_5$ a few times until reproducible pressure–composition diagrams are obtained. The hysteresis is initially large but is reduced substantially in subsequent cycles (significantly lower absorption and slightly higher desorption pressures) [1, 4].

There are three main microstructural alterations arising from activation: (1) the observed fracture of bulk samples into fine powders [1] ; (2) anisotropic line broadening in diffraction patterns taken from activated powders; and (3) the occurrence of many dislocations in activated samples as observed by transmission electron microscopy. The extensive fracturing of $LaNi_5$ single crystals which occurs during hydrogen loading/unloading is clearly connected with the origins of hysteresis during activation and repeated cycling. Structural investigations of the activated powder have resulted in differing and conflicting interpretations of the line broadening results (either particle size and/or microstrain broadening) using X-ray and neutron diffraction (ND)–Rietveld structure refinements [4–8]. The activation of single crystals of $LaNi_5$ by repeated cycling around the hysteresis loop until steady state conditions are attained results in powder particles with *c*-axis preferred geometry, as inferred from the relative intensity of $\{0\,0\,1\}$ reflections, in comparison to those for mechanically powdered material [4]. Anisotropic broadening of the $\{h\,k\,0\}$ reflections suggests that there may be a strong relationship between the fracture of single crystals, the formation and dynamics of defects, and the hysteresis during the activation process [4].

The principal objectives of the present study were to investigate the fracture phenomena and mechanisms of $LaNi_5$ specimens from two different sources, and to correlate these with the pressure hysteresis during activation and subsequent absorption/desorption cycles.

2. Experimental procedures

2.1. Alloy materials and characterisation procedures

$LaNi_5$ alloy specimens were obtained from two sources: Research Chemicals, Phoenix, AZ supplied alloy

* *Now at*: Department of Mechanical Engineering, University of Newcastle, Callaghan, NSW 2308, Australia.

0022–2461

TABLE I Experimental parameters for hydrogen loading/unloading of $LaNi_5$ alloys

Expt. no.	Alloy	Initial condition	H/M
1	A	s.c	0.035
2	A	s.c.	0.051
3	A	s.c.	0.06
4	A	s.c.	0.1
5	A	s.c.	0.23
6	A	s.c.	1.0
7	A	Polished s.c.	0
8	B	Polished s.c.	0
9	B	s.c.	0.06
10	B	s.c.	1.0

s.c. Single crystals

1241 with a stated composition of 32.44 wt % La (equivalent to a stoichiometry of $LaNi_{4.93}$); Hy-Stor, MPD Technology Corporation, NJ, alloy # 205 was obtained (with a stated nominal stoichiometry of $LaNi_5$). Specimens from the two sources will be denoted by A and B, respectively. The alloys were sufficiently coarse grained to allow single crystals to be mechanically isolated. The characterization and subsequent investigations used standard scanning electron microscopy (SEM), energy dispersive spectroscopy (EDS), wavelength dispersive spectroscopy (WDS), transmission electron microscopy (TEM) and X-ray diffraction (XRD) procedures. The principal difference between the as-received alloys was the presence of a minor second phase in A. The implications of this will be described below.

2.2. Hydriding procedures

A selection of as-received single crystals from both sources were activated partially by incomplete hydrogen loading up to H/M $\leq$ 0.06 (H/M is the hydrogen-to-metal ratio). Single crystals were also completely activated by cycling through four cycles to H/M ca. 1.0. A manometric hydrogen absorption technique was used. Here, a reference volume is filled with hydrogen gas to a chosen pressure; this was then allowed to equilibrate with the sample chamber of calibrated volume. The decrease (increase) in pressure in the combined reference and sample chambers, after allowing sufficient time for the system to attain quasi-stasis, can then be used to calculate the amount of absorbed (desorbed) hydrogen. The pressure in the sample chamber was increased (decreased) in a stepwise fashion and the H/M data were recorded at the conclusion of each step. Pressures were measured with the aid of an electronic transducer with a dynamic range from 0 to 1.5 MPa. Additional details of the apparatus and the methodology can be found elsewhere [9].

The structural changes to the single crystals of both A and B alloys after incomplete (H/M $\leq$ 0.06) and complete (H/M ca. 1.0) cycling at 30 °C were investigated with SEM/EDS/WDS/TEM/XRD. The experimental parameters are summarized in Table I and the specimen characterization summary is represented diagrammatically in Fig. 1.

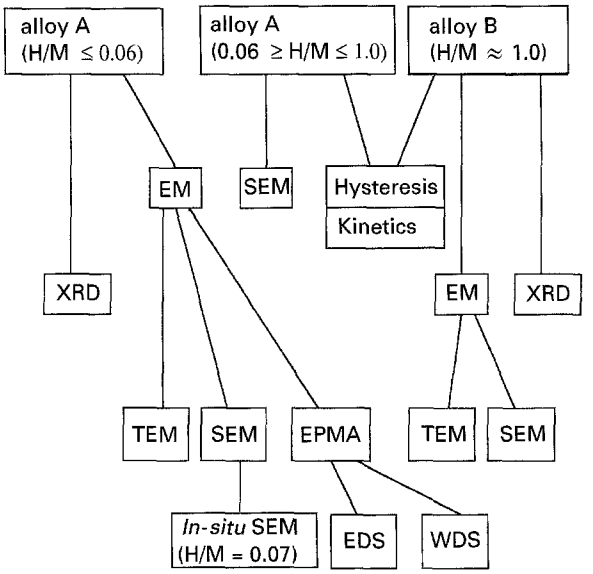

Figure 1 A schematic flow-chart of the experimental methodology.

3. Results

3.1. Specimen characterization

Detailed analyses of the as-received specimens of type A revealed the presence of nearly-parallel planar inclusions (apparent width < 6 μm and length ca. 1000 μm) and spherical inclusions (diameter ≤ 8 μm) as shown in Fig. 2. The average volume fraction of the minor inclusion phase was estimated at $6.3 \pm 1.1\%$, from point counting in backscattered electron images (BSI). However, the inclusion phase was not detectable by either TEM or XRD. The inclusions were analysed by EDS/WDS, and found to be a La-rich secondary phase of composition consistent with La_2Ni_7 stoichiometry. Alloy B, on the other hand, was single phase to within the resolution of the available techniques.

3.2. Fracture phenomena (H/M ca. 0.06)

The fracture induced by incomplete hydrogen loading of single crystals of type A (expt. no. 1–3) was in the form of splitting into flakes, as shown in Fig. 3a and b. It was found that the macroscopic cleavage process occurred ca. 30 min after the sample was removed from the reaction chamber and came in contact with air. It was associated with the production of moisture and traces of ammonia. Also shown in Fig. 3 are images which demonstrate that the cleavage mechanism is related to the presence of planar inclusions. Analysis by XRD of the flakes (expt. no. 1–3) showed a prominent [0 0 1] -preferred orientation; this is illustrated in Fig. 4a. Fig. 4b also shows, for comparison, results from Rietveld analysis of the XRD pattern of a well-activated type-A powder with random orientations. A single crystal specimen of type B was subjected to the same treatment (i.e. hydrogen loading to H/M ca. 0.06, expt. no. 9); in contrast, this specimen remained intact, with no visible signs of fracture.

3.3. Fracture phenomena (H/M = 1.0)

Hydrogen loading of single crystals or other bulk specimens (expt. no. 6) of either type produced extensive

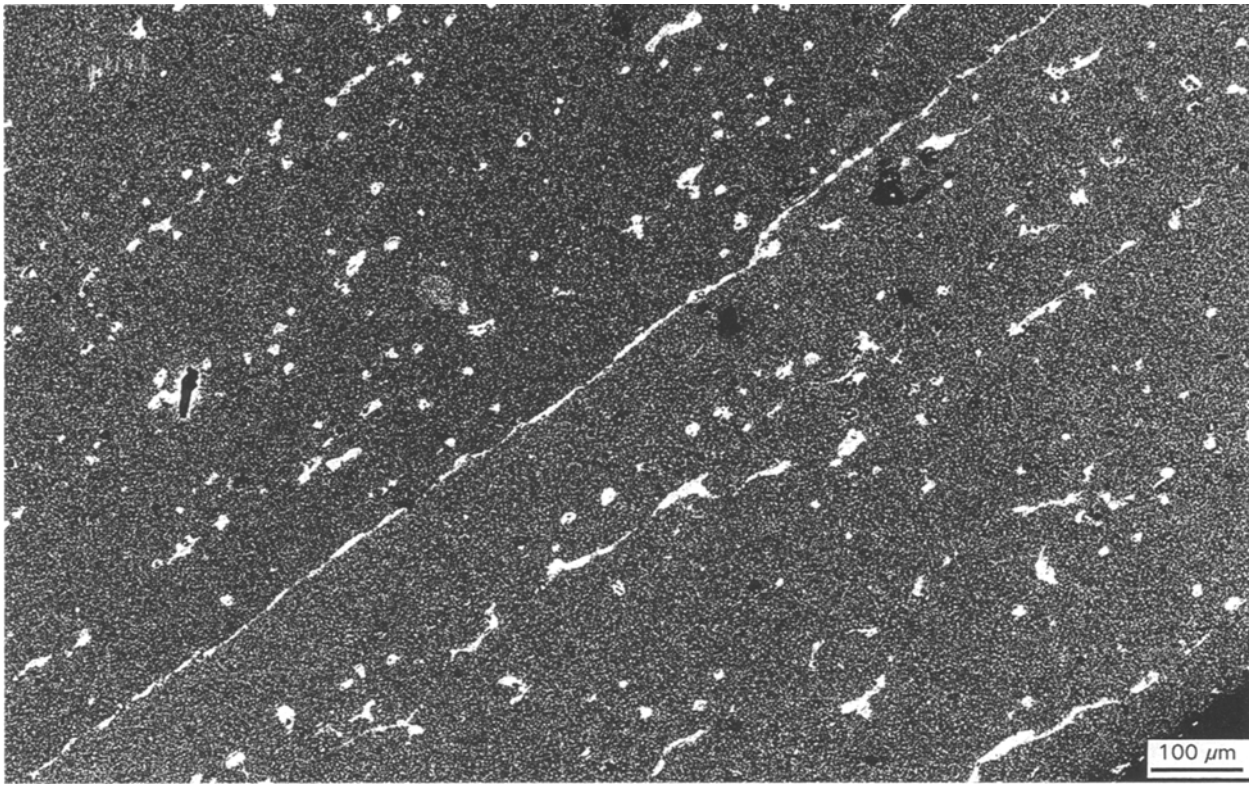

Figure 2 An SEM image (backscatter compositional) of a polished single crystal section of type A alloy. The texture of the planar and spherical inclusions is evident.

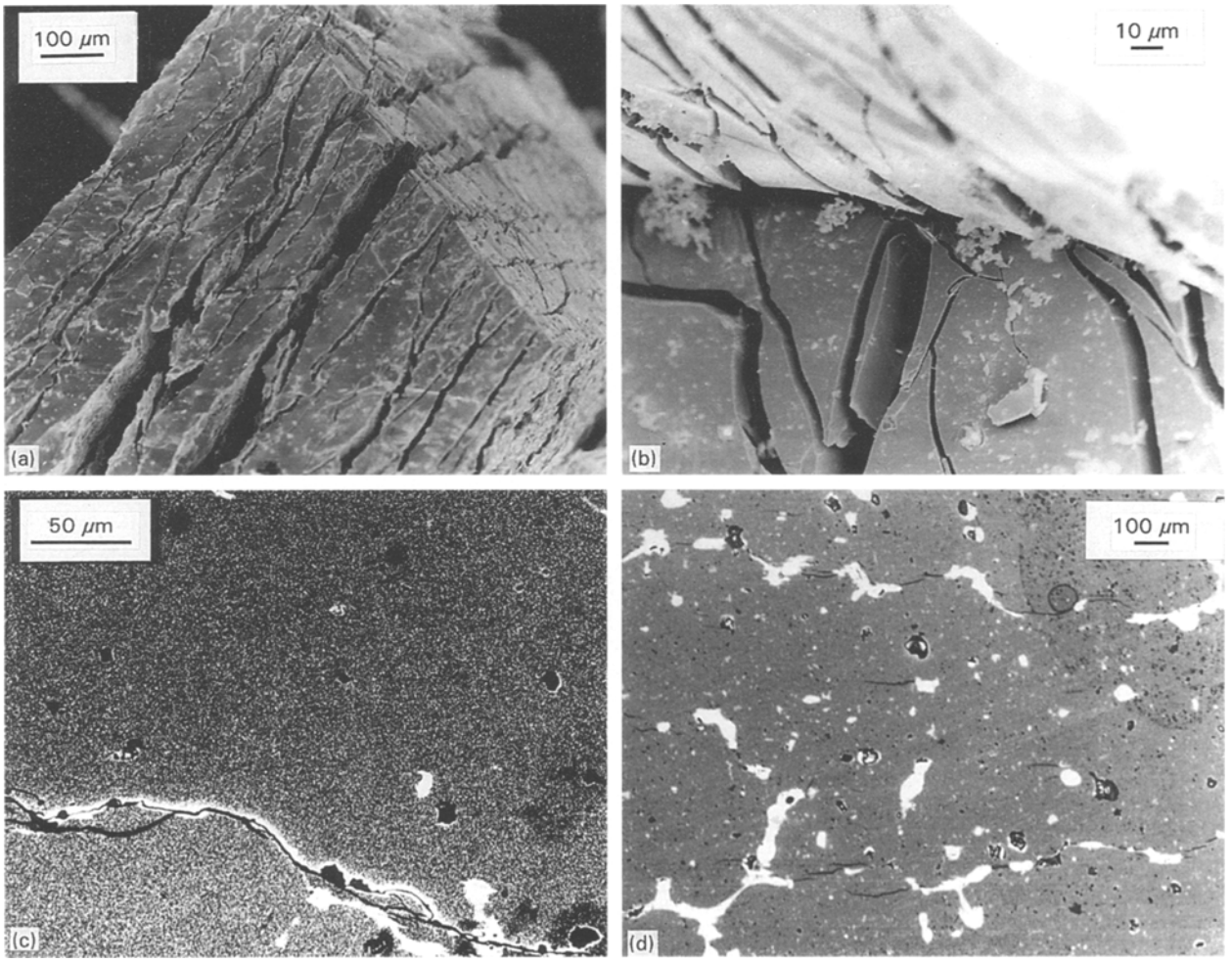

Figure 3 Complementary SEM images illustrating the preferred directions of cleavage of type A alloy at low hydrogen loading (H/M ca. 0.06). The micrographs illustrate extensive cracking in a single crystal to form flakes [(a) and (b)], and the relationship between the planar and spherical inclusions and the propagation of cracks [(c) and (d)].

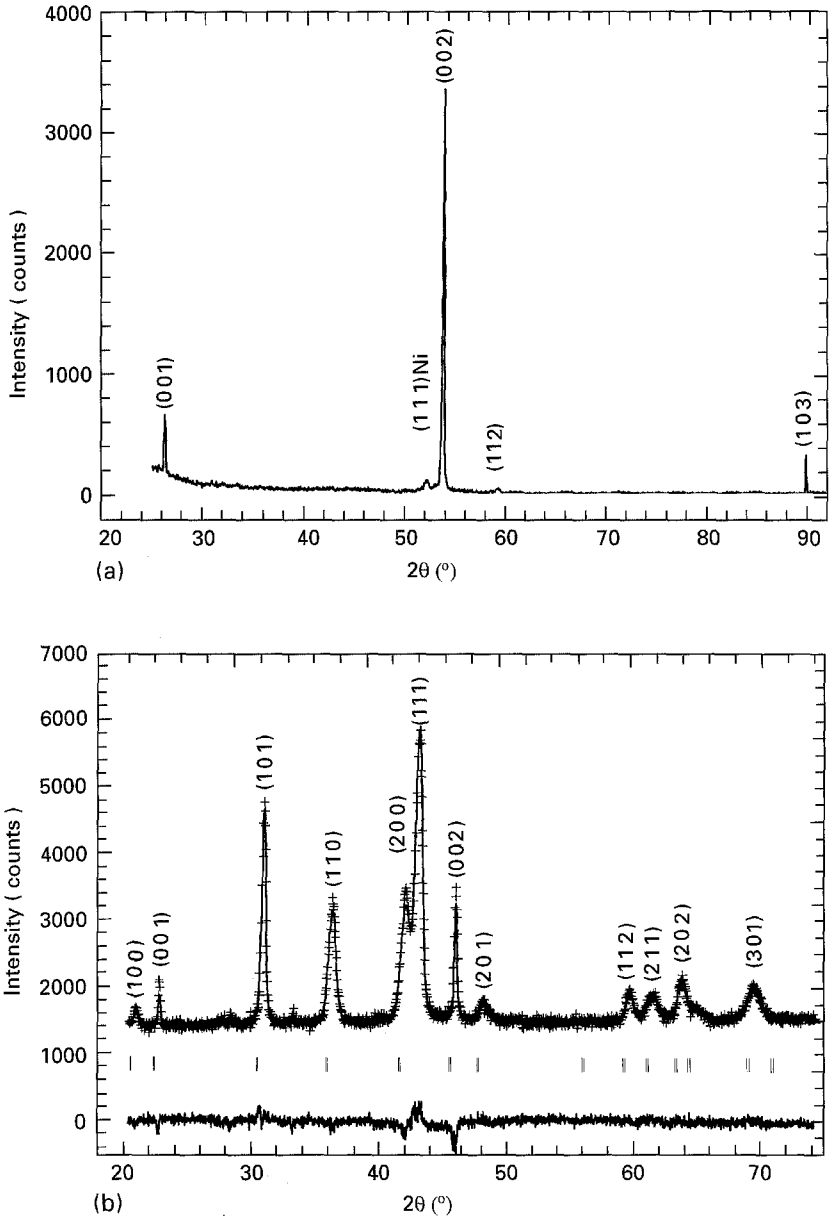

Figure 4 (a) A Co K_α XRD scan of the flakes resulting from fracture of type A alloy at low hydrogen loading (H/M = 0.046) during the first cycle. Note the strong (0 0 0 1) preferred orientation. The reflection at 52.10° originates from the Ni specimen holder. (b) Data from XRD analyses, using CuK_α radiation, of a fully activated (i.e. cycled several times) powder specimen showing nearly random orientation. Rietveld analysis was carried out: the calculated profile is shown as a superimposed curve on the raw data (+). The difference trace and the reflection positions are also indicated.

fracturing with an intricate network of fine, randomly oriented cracks; this is illustrated in the SEM image in Fig. 5. Thus, the fracture of single crystals of alloy A occurs in two stages (major parallel cracking into sheets, at low-hydrogen loading, and minor cracking transverse to the sheets, at high loading), while type-B specimens exhibit only a single stage (at high-hydrogen loading).

3.4. Activation and hydriding properties of alloys A and B

The results as pressure versus hydrogen-to-metal ratio from several complete hydriding/dehydriding cycles are shown in Fig. 6 for alloys of both types. Table II lists the pressures of absorption and desorption, measured at the midpoint of each plateau (i.e. for H/M = 0.5). Also given, as a measure of the extent of hysteresis, are the differences between these pressures in linear and Gibbs free-energy units, $\Delta G = RT \log(p_{ab}/p_{de})$, where p_{ab} and p_{de} are the absorption and desorption plateau pressures, respectively, both measured at H/M = 0.5. It is immediately obvious that the relatively large pressure hysteresis of the first cycle decreased substantially in subsequent cycles, and approached steady-state values after a few cycles.

3.5. Kinetic properties of activated alloys A and B (H/M ca. 1.0)

The kinetics of the fully activated alloys A and B, taken as the rate of hydrogen absorbed over 5 h, were identical, suggesting that the kinetics of activated materials were not affected by the nature of the microstructure of the alloy. The implication was that equal amounts of lattice damage had occurred in both alloys.

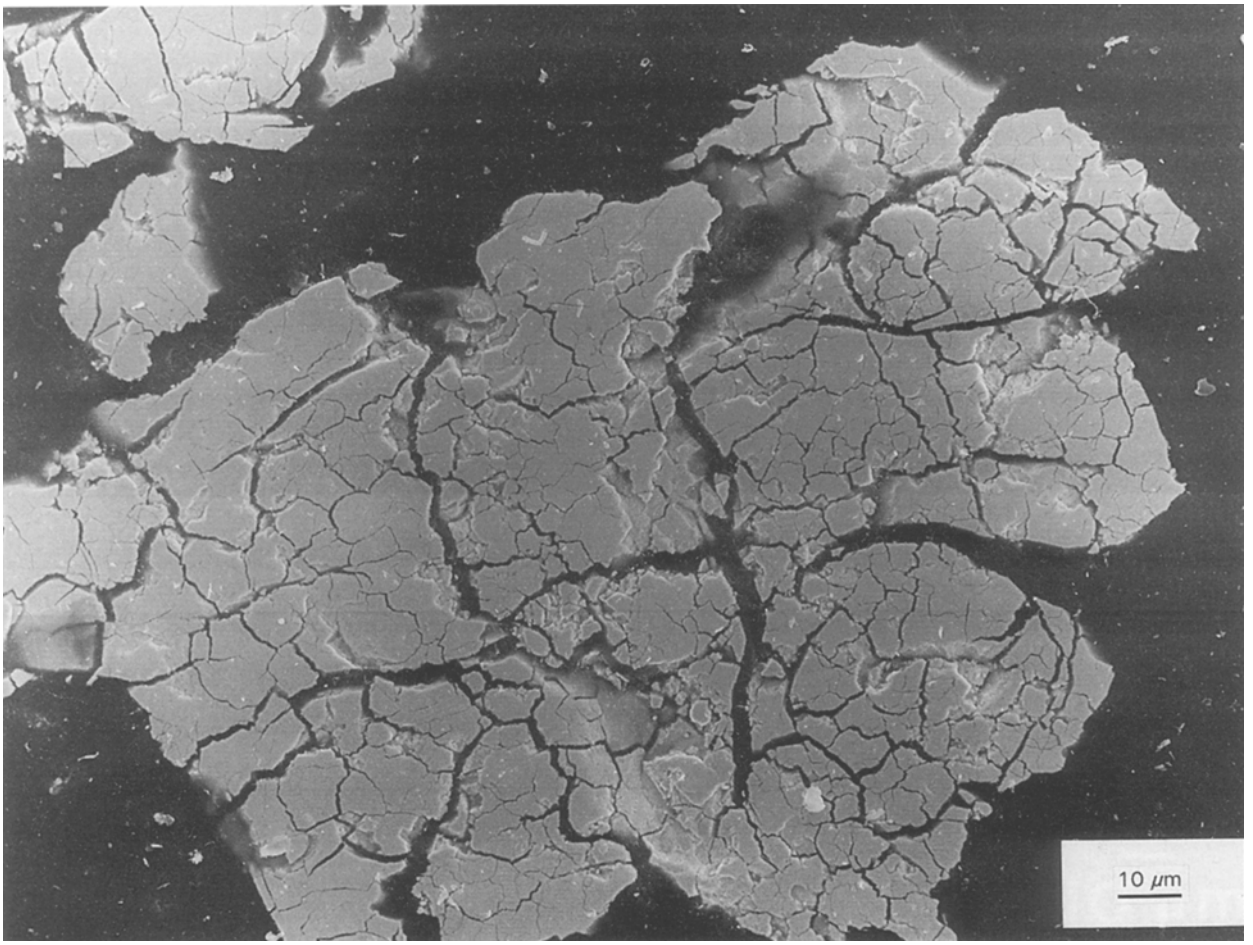

Figure 5 An SEM micrograph showing the transverse fracture of the powder of alloy A after loading to a high H/M ratio.

4. Discussion

4.1. Fracture mechanisms

The measured compositions of the inclusions in alloy A were consistent with these being an intermetallic alloy of La_2Ni_7 stoichiometry. Inclusions appear to occur as layered sheets orientated perpendicularly to the *c*-axis of the host $LaNi_5$ hexagonal crystal structure. Examination of the La–Ni phase diagram shows that this phase will form in alloys somewhat deficient in Ni; phase separation is promoted if the alloy is cooled slowly from 1350 to 1000°C [10]. The preferred orientation of the planar inclusions is presumably due either to the growth of the host single crystal in the *c*-direction and/or to a better match of lattice parameters at the *a*–*b* plane interface.

Single crystals of alloy A were observed to fracture into flakes at low hydrogen loading with preferred {0 0 1} planar orientation; it seems likely that there is a connection with the planar inclusion phase oriented perpendicularly to the *c*-axis of the $LaNi_5$ unit cell. Incomplete hydrogen loading (H/M ca. 0.06) results in the expansion of the $LaNi_5$ lattice in the basal plane, thus forming the α-phase. Assuming that the inclusion phase does not take up hydrogen to the same extent as the host metal at the same pressures, stresses will be generated at the interface by the increasing mismatch between the α-phase and the planar inclusions. The result is delamination at the inclusion boundaries; the sequence of events is illustrated in Fig. 7. Additional long-range cleavage takes place in alloy A when unlinked planar inclusion-phase regions are bridged due to the stresses created by higher hydrogen loadings (this was demonstrated in expt. no. 7, and illustrated in Fig. 3d). Thus, cracks readily propagate through the alloy along the planar inclusions causing more extensive damage than would be occasioned by the presence of only spherical inclusions. Cracks initiated at a spherical inclusion can only propagate as far as the perimeter due to the lack of connecting pathways.

The fracture of type B alloy, as well as the second stage fracture of type A, associated with higher hydrogen loadings, is due to a different mechanism. The relative expansion along the *a*- and *c*-axes is identical during the α↔β phase transformation. Also, it has recently been confirmed, with neutron diffraction, that α and β domains coexist in the same particles of the material [11]. Stresses are created at the boundaries between the α- and β-phase regions due to the lattice mismatch and result in crack initiation. This is shown schematically in Fig. 8. At a more detailed level we might note that the lattice mismatch at the phase boundaries generates defects (dislocations) which may propagate, resulting in delocalized strain throughout the alloy. After several hysteresis cycles, the net production of dislocations will approach zero and the alloy approaches steady-state kinetics and hysteresis. This picture agrees with a proposed mechanism for activation [4].

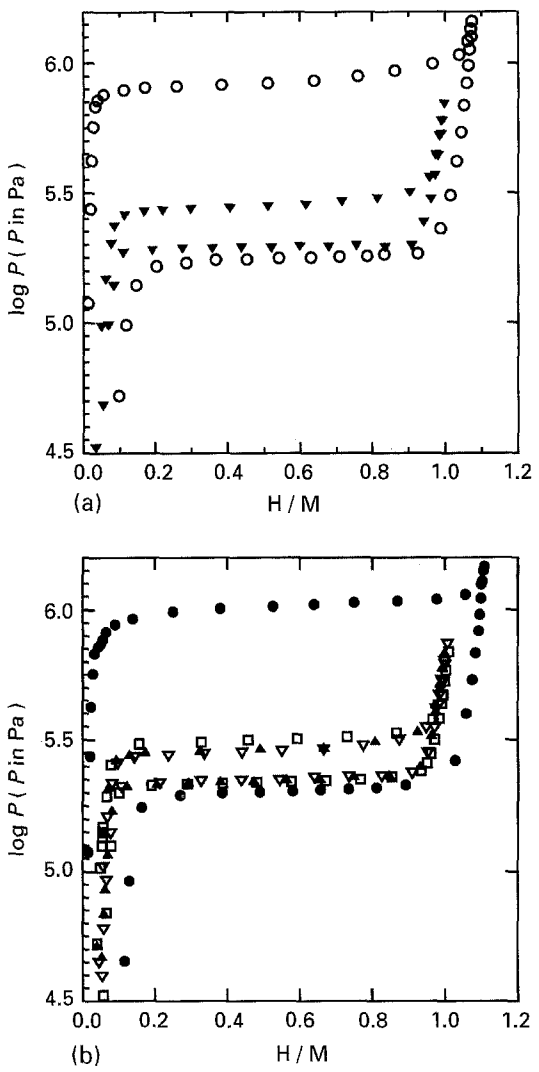

Figure 6 The hysteresis curves, showing log P versus H/M of alloys A (upper) and B (lower). The symbols refer to: alloy A: (○) first cycle, (▼) fourth cycle; alloy B: (●) first cycle, (□) second cycle, (▲) third cycle, (▽) fourth cycle. The shifts at the end-points between the first and subsequent cycles are possibly related to the formation of a "decomposition" layer (this has been the subject of a companion study to be reported elsewhere).

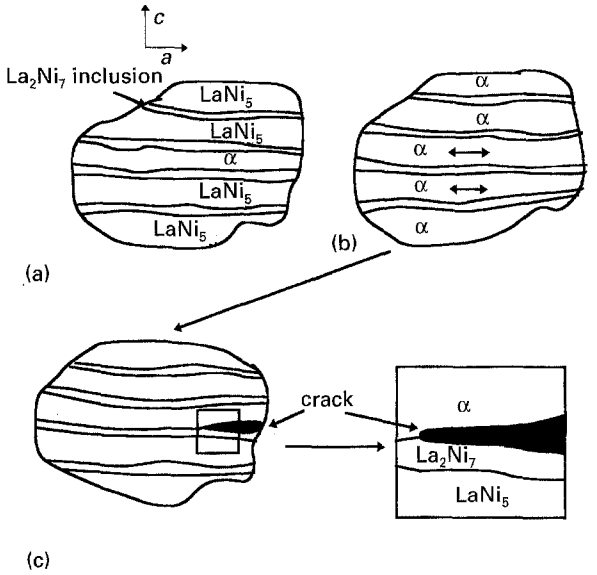

Figure 7 A schematic representation of a model describing laminar fracture at the inclusion boundaries between the planar inclusions and the $LaNi_5$ matrix. The following sequence is envisaged: (a) preferential absorption of hydrogen by the host matrix; (b) the α-phase expands in the basal plane; (c) nucleation of cracks by accumulated stresses and propagation along the inclusion–matrix interface.

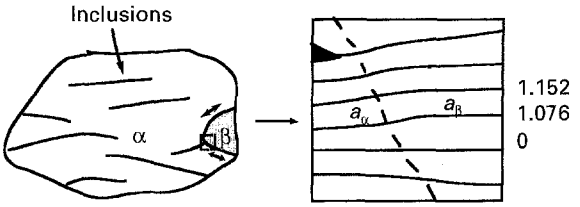

Figure 8 A schematic representation of a model for the fracture at high hydrogen loadings. This model, with minor alterations, has validity for both alloys A and B. The model requires the coexistence of microdomains of the α-and β-type hydride phases, where a_α and a_β are the lattice constants for the respective phases. The strains resulting from the linear expansions (7.6% per unit cell) with respect to a reference plane (0) are shown in an enlarged view. The outcome is fracture along the inclusion–matrix interface as well as throughout the alloy.

4.2. Effects of fracture on hydriding properties

Alloy B exhibits far greater pressure hysteresis than alloy A during the first cycle, but both arrive at similar asymptotic steady state conditions after the fourth or fifth cycle (see Fig. 6). This would suggest that the differences in the pressure hysteresis between the two alloys during the first few cycles are related to the presence of planar inclusions in alloy A, and their absence in alloy B. The presence of planar inclusions in alloy A will reduce the resistance of the alloy to hydrogen absorption during the initial cycle if the inclusions are sites of fracture initiation at low stresses. Thus, the promotion of fracture may result in greater hydrogen uptake due to the higher specific surface area of clean metal exposed to hydrogen (a kinetic effect); the fracture may also influence the defect concentration and hence lower the hysteresis. After

TABLE II Pressures of absorption and desorption measured at H/M = 0.5. A measure of the extent of hysteresis is indicated by the differences between these pressures in linear units of kPa and Gibbs free-energy units, ΔG in kJ

Cycle	Absorption (kPa)		Desorption (kPa)		Hysteresis (kPa)		Hysteresis (kJ)	
	A	B	A	B	A	B	A	B
1	838	1025	176	198	662	828	1707	1800
2	–	316	–	216	–	100	–	416
3	–	289	–	218	–	71	–	308
4	281	284	195	221	86	63	400	274

activation, alloys A and B both exhibit reproducible and near-identical pressures of the absorption plateau (at H/M ca. 0.5), indicating that the major microstructural barriers to hydrogen uptake are overcome during the initial cycle, after which further fracture and net defect production is minimal. This argument is supported by the observed equivalence in the distribution of strains [the anisotropic line broadening is the same ($\Delta a/a = 0.96$) for both alloys after four cycles [12]] and on the observation that the kinetics for both alloys A and B are identical within experimental resolution.

The activation of alloys A and B is arguably an energy-driven process whereby it becomes progressively energetically more difficult for hydrogen atoms to access crystallographically non-equivalent interstitial sites. This is manifest in measurements of the pressure versus hydrogen concentration as a distinct slope of the pressure 'plateaux', representing the range of interstitial site energies. The slopes of the absorption plateaux [$\Delta \log p/\Delta(\mathrm{H/M})$] are the same for both alloys implying the same range of site energies. The earlier fracture of alloy A, at H/M ca. 0.05, in comparison to H/M = 0.15 for alloy B, suggests that the additional surface area created by the fracture at the planar inclusions in alloy A promotes greater hydrogen absorption and faster kinetics in alloy A during the first cycle. The fracture of alloy A lowers the plateau pressure, during the first hydrogen loading cycle, by $\log p$ ca. 0.1, in comparison with that for alloy B (see Fig. 6). This may mean that the plateau points for alloy B in the first cycle are less representative of true steady-state conditions than the points on the alloy A curve. Alternatively, the free energy required to populate sites in alloy A may be genuinely lower by an amount equivalent to $\Delta \log p$ ca. 0.1. We feel that the former explanation of a kinetic influence is more plausible, in comparison with the activation-driven mechanism; the fracture of alloy A at low hydrogen loading is more likely to facilitate the attainment of steady state than to alter the activation energies by amounts comparable to the difference between those for "easy" and "hard" interstitial sites (i.e. the absorption plateau slope).

5. Conclusions

The present study shows that the phase structure of $LaNi_5$ affects the hydriding properties during the early stages of activation. The adventitious phase separation of one alloy is found to promote an anisotropic fracture process, thus lowering the hysteresis during the first hydrogen loading/unloading cycle, as well as improving the kinetics of hydrogen uptake. Both of these factors are clearly relevant for the technical attractiveness of $LaNi_5$ as a practical hydride. The implication is that judicious tailoring of the material's microstructure can change the initial phase structure and thus enhance the hydriding characteristics. This is seen as a promising area of study warranting further research.

Acknowledgements

This project was funded in part by the Australian Research Council. Theodora Kastrissios wishes to acknowledge the support of an APRA scholarship. We acknowledge additionally support from and useful consultations with Evan M. Gray and Craig Buckley.

References

1. H. H. VAN MAL, *Philips Res. Rep., Suppl.*, **1** (1976) 1.
2. T. B. FLANAGAN and J. D. CLEWLEY, *J. Less-Common Met.*, **83** (1982) 127.
3. J. R. LACHER, *Proc. R. Soc. A.*, **161** (1937) 525.
4. E. H. KISI, C. E. BUCKLEY and E. M. GRAY, *J. Alloys and Compounds*, **185** (1992) 369.
5. C. LARTIGUE, A. PERCHERON-GUEGAN, J. C. ACHARD and J. L. SOUBEYROUX, *J. Less-Common Met.*, **113** (1985) 127.
6. C. LARTIGUE, A. LE BAIL and A. PERCHERON-GUEGAN, *J. Less-Common Met.*, **129** (1987) 65.
7. P. FISCHER, A. FURRER, G. BUSCH and L. SCHLAPBACH, *Helvetica Physica Acta*, **50** (1977) 421.
8. A. L. BOWMAN, J. L. ANDERSON and N. G. NERESON in Proceedings of the 10th Rare Earth Research Conference, Arizona, 1973, edited by C. J. Kevane and T. Mueller, p. 485.
9. C. E. BUCKLEY, PhD thesis, Griffith University, Australia (1993).
10. "ASM handbook – alloy phase diagrams", Vol. **3** (The Materials Information Society, USA, 1992).
11. E. H. KISI, E. M. GRAY and S. J. KENNEDY, *Alloys and Compounds*, **216** (1994) 123.
12. T. KASTRISSIOS, MPhil. thesis, Griffith University, Australia (1993).

Received 14 April 1994
and accepted 5 April 1995